Il progetto Cabianca

# Networking Analysis of Photonics Integrated Multiband WSS Based ROADM Architecture


Muhammad Umar Masood
*Politecnico di Torino, IT*
muhammad.masood@polito.it

Ihtesham Khan
*Politecnico di Torino, IT*
ihtesham.khan@polito.it

Lorenzo Tunesi
*Politecnico di Torino, IT*
lorenzo.tunesi@polito.com

Bruno Correia
*Politecnico di Torino, IT*
bruno.dearaujo@polito.it

Rasoul Sadeghi
*Politecnico di Torino, IT*
rasoul.sadeghi@polito.it

Enrico Ghillino
*Synopsys, USA*
enrico.ghillino@synopsys.com

Paolo Bardella
*Politecnico di Torino, IT*
paolo.bardella@polito.it

Andrea Carena
*Politecnico di Torino, IT*
andrea.carena@polito.it

Vittorio Curri
*Politecnico di Torino, IT*
curri@polito.it



***Abstract*—Due to increasing traffic demand, the current optical transport infrastructure is experiencing capacity problems. Spatial Division Multiplexing (SDM) and Bandwidth Division Multiplexing (BDM) have emerged as potential solutions to increase the capacity of the network infrastructure. In this paper, a novel modular photonic integrated multiband wavelength selective switch (WSS) in a reconfigurable optical add-drop multiplexer (ROADM) architecture is proposed. This proposed WSS can operate over a wide spectral range, including S+C+L bands, and is potentially scalable to a large number of output fibers and routed channels while maintaining a small footprint. We investigated the network performance of the proposed multiband WSS switching structure in the Spain-E topology network and performed a detailed comparison for the SDM and BDM scenarios. In comparison to the SDM approach, which requires the deployment of additional fibers, the results show that the cost-effective BDM scenario can utilize the capacity better without installing the new fiber infrastructure or using dark fibers.**



***Index Terms*—Multiband, Wavelength Selective Switch, Photonic Integrated Circuit, High-capacity Optical Networks**


## I. Introduction

The deployment of 5G and high-capacity optical access networks will put a strain on telecommunications infrastructures [1]. This requires service providers to implement cost-effective, scalable, and flexible solutions to increase the capacity of existing infrastructure. Modern optical transport nowadays is usually based on transparent propagation of Wavelength Division Multiplexing (WDM) channels using coherent optical technologies with dual polarization over the entire C-band in a spectral window of 4.8 THz, enabling a maximum transmission capacity of about 38.4 Tbps per fiber while using PM-16QAM [2]. Further increasing network capacity will require solutions that scale the technology currently in-use or implement new ones. The most feasible options for improving the available capacity of optical networks are (a) spatial division multiplexing (SDM) , an approach that can be implemented with multicore (MCF), multimode (MMF) or multi-parallel (MPF) fibers, and (b) Band-division multiplexing (BDM), which uses a wider spectral range of the fiber to enable transmission over the entire low-loss spectrum of optical fibers (e.g., 54 THz in ITU G.652.D fibers).

The SDM solutions available today rely on the availability of dark fiber or the installation of new fiber. This approach replicates the established technology that has been applied over the years for C-band line systems. The other SDM solutions (e.g., MMF and MCF) have the potential for higher capacities. However, they require a complete replacement of the optical transport infrastructure, which requires a significant CAPEX effort. On the other hand, BDM uses the unused spectral portion of the fiber and aims to transmit WDM channels over the entire available low-loss spectrum, from the O to the L band (1260-1625 nm), and offers a potentially available frequency bandwidth of over 50 THz [3]. BDM is a potentially low-cost solution with the ability to increase the capacity of the existing network infrastructure. The primary issue lies in optical amplification: e.g., the technology is not yet established in some spectral bands. Amplifier prototypes that operate in the extended-spectrum range are now available commercially [4]. The BDM technique also requires enabling transparent wavelength routing by the filtering and switching modules. The fundamental component of the WDM switching architecture is that the WSS, which provides independent control and routing of every input channel to a fiber output. Typically, WSS is implemented using microelectromechanical mirrors (MEMS) and liquid crystal on silicon (LCoS) technology, resulting in devices that are typically bulky and complex to manufacture and maintain [5].

This work proposes a multiband WSS implementation using rapidly emerging photonic integrated circuits (PIC) technology, which offers a low-cost solution with a small footprint and large production capacity. The proposed WSS has a modular architecture that can operate in a wide range of the optical spectrum covering the S+C+L bands. The design of the proposed WSS enables scalability for more output fibers and a large number of channels with a smaller footprint than conventional MEMS-based solutions. In this analysis,

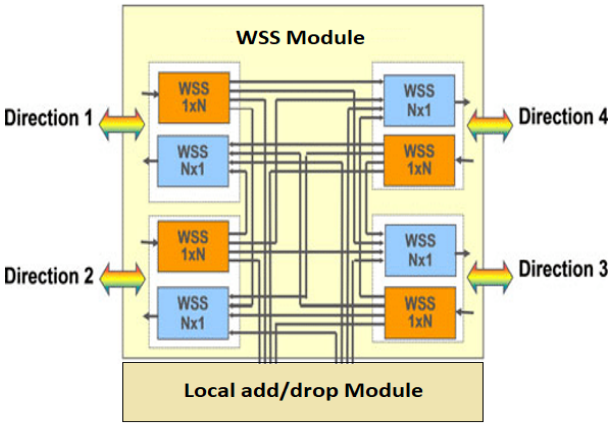


Fig. 1. ROADM architecture enabled by WSSs.

only the switching functionality of the ROADM architecture (WSS module) is considered without taking into account the local add/drop module of the ROADM, shown in Fig. 1. A detailed evaluation of the network performance of the proposed ROADM architecture based on the new multiband WSS is also demonstrated, applying the study to the Spain-E network and comparing SDM and BDM solutions.

## II. Wavelength Selective Switch Architecture

The proposed architecture offers a fully integrated solution enabling wavelength-selective switching in a WDM multi-band application scenario. All the internal components of the architecture have been implemented as PICs, targeting the three main bands of interest, namely the S+C+L optical windows. The architecture allows independent routing of each input channel toward the target output port, avoiding routing conflicts and minimizing the inter-channel and inter-band crosstalk. Regarding the transmission scenario, the demultiplexing operation has been tailored for a 100 GHz Free Spectral Range (FSR) comb.

The proposed structure is depicted in Fig. 2, highlighting the different operational stages required to achieve the WSS operation: the architecture can be divided into two main stages, the first tasked with channel separation, and the second with the switching and routing toward the target output port. This stages can be further divided into their internal block components, which will be described and characterized in the following sections.

### A. Filtering Section

The first section is tasked with achieving the required demultiplexing operation, separating each individual channel of the input signal into a separate waveguide. This operation is achieved through a cascade of different filtering stages, which are designed to reduce and contain the losses as well as the channels crosstalk. The main issue affecting photonic integrated filtering structures is the periodicity of the frequency response in interference-based solutions: this lead to an issue in both the operating bandwidth as well as the resolution capabilities for dense WDM applications. In order to mitigate

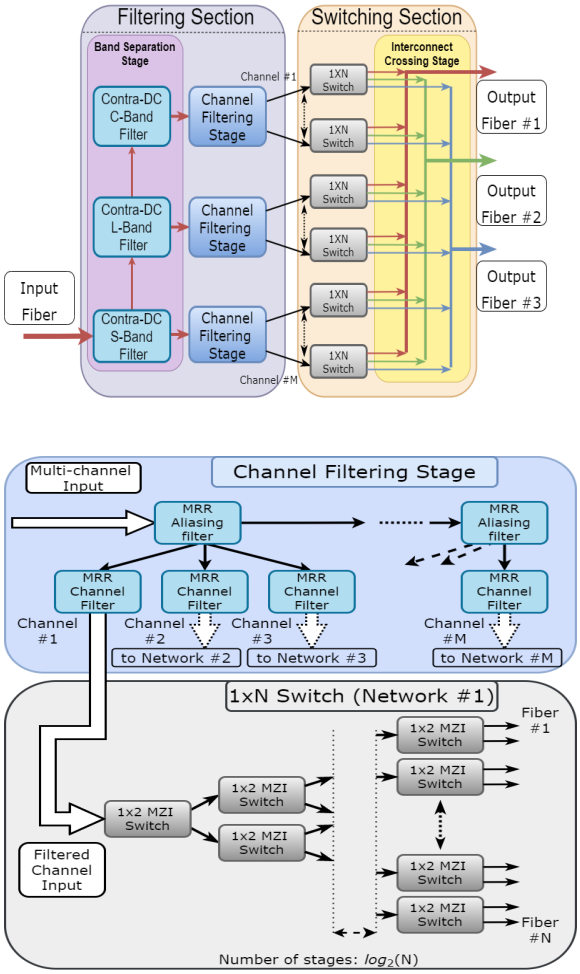


Fig. 2. Circuit model of the proposed WSS structure, highlighting the main operational stages and their block structure.

the aliasing issue two different components are deployed in the filter cascade.

To begin with, the three bands of operation (S+C+L) are separated, avoiding severe inter-band interference in the later stages, while the second section of the filtering stage isolates each channel. This is achieved through two main structures, namely Contra-Directional Couplers (CDC) and Micro-Ring Resonator (MRR) filters. The CDC structures, shown in Fig. 3, have been designed through Coupled-Mode Theory (CMT) [6]: by adjusting the grating pitch, period and chirp a flat and wide-band response can be obtained, allowing the separation of the S+C+L bands. This solution is unfortunately unsuitable for the individual channel separation, as CDC structures have a large foot-print and cannot offer the required sharp transition at the desired channel bandwidth. As such the later section of the filtering stage is implemented through a two-stage ladder MRR based filter, shown in Fig. 4. These structure can be designed to achieve a flat-top filtering response, with a steep stop-band transition and attenuation, ideal for the target application. Unfortunately, as previously stated, interference-based solutions suffer from an aliasing issue due to the period nature of the response. This issue

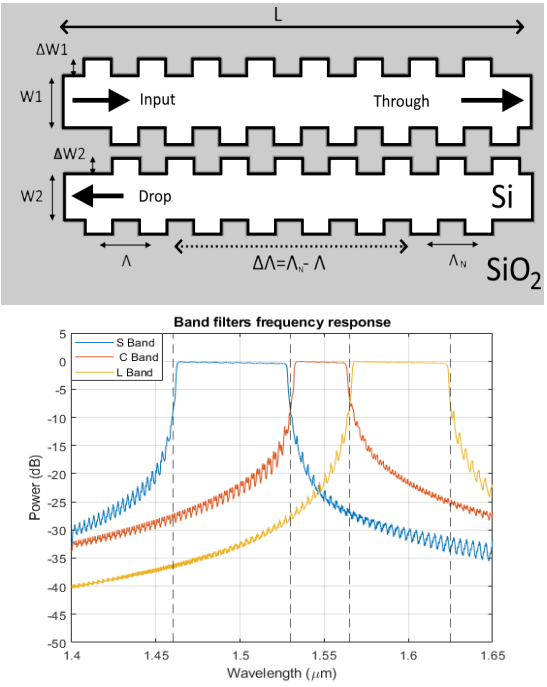


Fig. 3. Contra-Directional Coupler filter: (top) schematic and (bottom) frequency response.

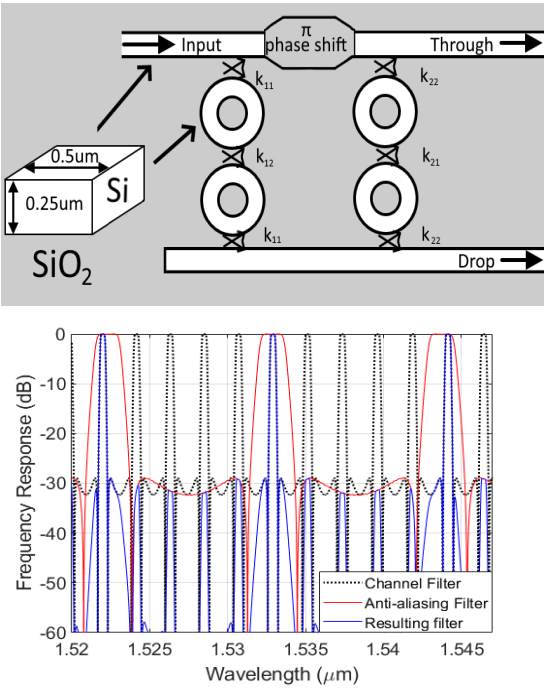


Fig. 4. Device schematic for the two-stage ladder MRR filter. The frequency response is shown for the individual device together with the proposed anti-aliasing solution.

can be mitigated by cascading multiple filtering elements with different response periodicity: the larger band device acts as an anti-aliasing filter, allowing the extension of the WDM comb that can be handled by the device.

### *B. Switching Section*

After the filtering stage, which separates the individual channels, the following section is tasked with routing the

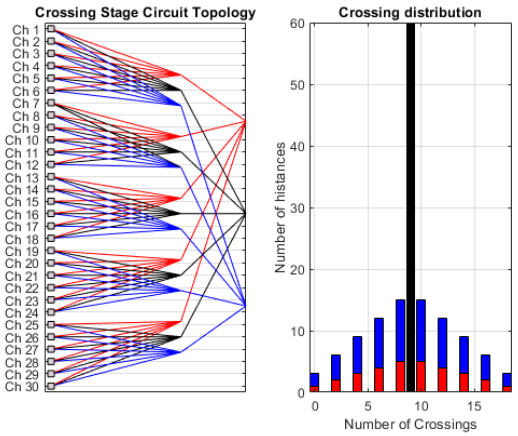


Fig. 5. Interconnect stage topology and distribution of the encountered number of waveguide crossing by each channel.

signals to the target output port. This operation is achieved through independent parallel $1\times$N switching networks, depicted in Fig. 2. These structures are designed starting from a fundamental $1 \times 2$ Optical Switching Element (OSE), which can be used as a template to achieve the desired switching capability. In this analysis the OSE has been implemented as a Mach-Zehnder Interferometer (MZI) switch, which represents a typical integrated solution for frequency-independent switching [7]. MZI can achieve a large flat band of operation [8] , while being easily tailored to the target central frequency of interest. The switching operation is achieved through thermal control of the arms of the MZI structure, which enables a low-loss and crosstalk symmetric response for both switching states. After the switching operation, each channel is then routed to the correct output port through a waveguide crossing layer, which is simply a topological representation of the interconnect structure. In this section each waveguide crossing has been considered as an ideal lossy element, introducing a flat loss of $0.045\,\mathrm{dB}$ across the whole spectrum.

## III. WDM Transport Layer

The proposed architecture has been tested in a coherent transmission scenario, considering a target application with a $100\,\mathrm{GHz}$ spaced WDM comb with 10 channels in each of the S+C+L bands (30 total channels). The channels and the transmission impairment are simulated for a dual-polarization 16-QAM modulation scheme, with symbol rate $R_s = 60$ GBaud, as defined in the 400ZR standard [9]. Each internal component discussed in the previous section has been simulated in the Optsim Photonic Circuit Simulation Suite, deriving the circuit blocks used for the transmission level simulation. The optical signal to noise ratio (OSNR) penalty ($\Delta$OSNR) has been taken as the QoT metric, extracted for a Bit-Error Rate (BER) reference $\mathrm{BER_{th}} = 10^{-3}$.

Two main components of the penalty can be isolated from the obtained results: a path-dependant component, due to the encountered number of waveguide crossing, and a path-independent component, due to the filtering and switching elements. This result, coherent with the modelling of the

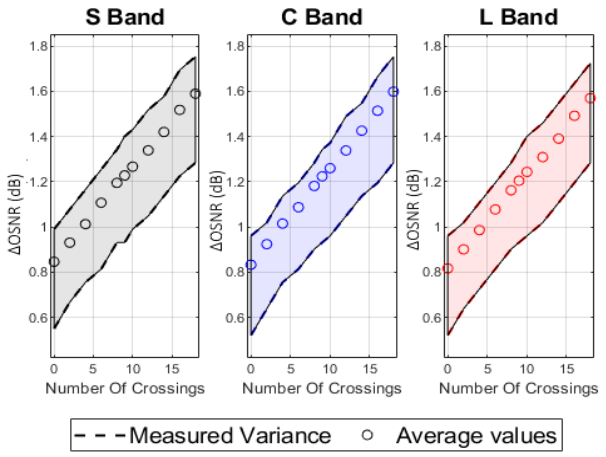


Fig. 6. ΔOSNR penalty distribution for the 10 test channels over the S+C+L bands.

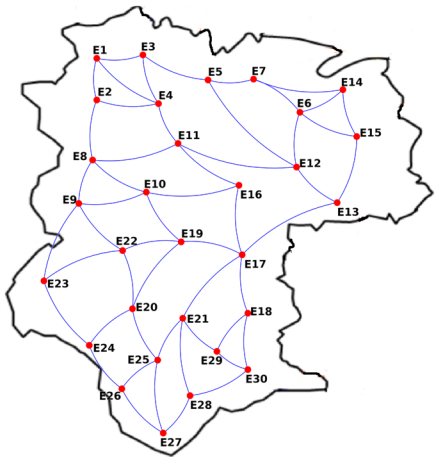


Fig. 8. Spain-E topology.

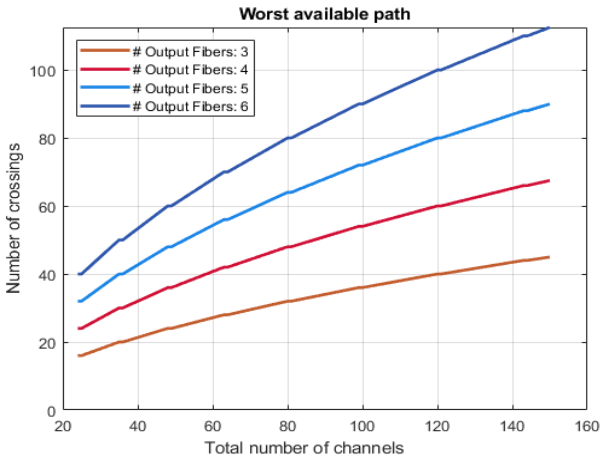


Fig. 7. Number of crossing in the worst path as a function of the number of input channels and number of output fibers (# Output Fibers).

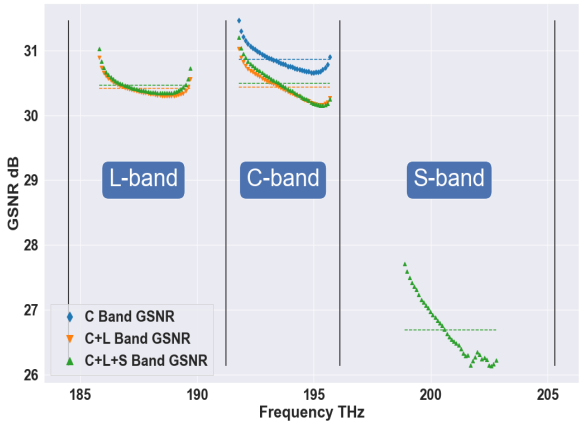


Fig. 9. GSNR vs. frequency for all channels evaluated in each band for all scenarios (C-band only, C+L and C+L+S).

architecture, allows to evaluate the penalty as a function of the routing, taking into account the crossing topology of the interconnect stage. The topology for the case study under-analysis is depicted in Fig. 5, which highlight both the overall structure of the stage, as well as the distribution of the number of crossings for all the routing configurations available in the device. By plotting the penalty as a function of the encountered crossings, as shown in Fig. 6, the trend shows relative comparable results in the three target bands: both the average penalty and the variance are compatible, highlighting the optimized design for the components in each of the bands. Due to the comparable results, as well as the penalty strong dependence on the number of crossings with respect to the path-independent component, the proposed model has been used to estimate the performances and scalability on different parameters sizes (number of output ports and number of total channels). One figure of merit that can be considered as the scalability metric is the number of crossings encountered in the worst available routing path, as depicted in Fig. 7: this value does not represent the distribution of the average penalty encountered by the different channels, although can be considered as the worst-case bound in terms of Quality of Transmission (QoT) impairment.

This topology-based abstraction of the device can be considered a reasonable trade-off between accuracy and computational or time feasibility. While the time-domain evaluation of the full system yields an accurate results based on the actual implementation size of the WSS, the computational cost makes the accuracy less significant. Due to the abstraction of the components required for the system-level simulation, a more accurate digital signal processing (DSP) simulation is less meaningful, due to the underlying necessary simplification of the models at the device level. As such the topology-based abstraction for the penalty evaluation is considered valid for the purpose of system-level analysis, allowing a scalable model based on the DSP time-domain results of the case study.

## IV. Network Performance Analysis

To analyze the impact of the new WSS architecture on different optical transport solutions, we studied the network's overall performance. We used the Statistical Network Assessment Process (SNAP) [10], which operates on the physical layer of the tested network and is based on the degradation in the QoT caused by each element of the network. In this

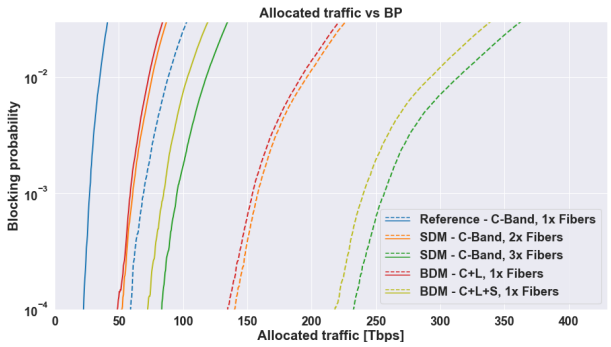


Fig. 10. Blocking probability evaluated over the Spain-E network considering ideal(....) and ZR+(—) transceivers case.

case, the QoT metric is the generalized signal-to-noise ratio (GSNR) calculated considering both $P_{\mathrm{ASE}}$ and $P_{\mathrm{NLI}}$, using

$$\mathrm{GSNR_i} = \frac{P_{\mathrm{S,i}}}{P_{\mathrm{ASE}(f_i)} + P_{\mathrm{NLI,i}}(f_i)}\,, \tag{1}$$

for the $ith$ channel with center frequency $f_i$, where $P_{\mathrm{S,i}}$ is the transmitted power of the signal, $P_{\mathrm{ASE}(f_i)}$ is the amplified spontaneous emission, and $P_{\mathrm{NLI,i}}(f_i)$ is the non-linear interference of the fiber.

We assume that a multiband optical system is built from a series of bands, with components, especially optical amplifiers, optimized for each band [3]. Thus, we assume that each fiber in the amplified lines has identical lengths of 75 km, and the fiber types used are standard single-mode fiber (ITU-T G.652D). We assumed commercially available erbium-doped fiber amplifiers (EDFAs) for C- and L-band channels and thulium-doped fiber amplifiers for the S-band [11]. Each band operates on the ITU-T 100 GHz WDM grid with transceivers tuned to a symbol rate of 60 Gbaud. For the C, L and S bands, an input power optimization was performed for the 40 channels of each band, following a span-by-span strategy using the local optimization global optimization (LOGO) algorithm based on maximizing QoT [12]. The GSNR profile of a fully loaded single span of 75 km with respect to frequency for the scenarios C, C+L, and C+L+S is shown in Fig. 9. The mean GSNR determined with reference to the LOGO optimization is shown with dashed lines. In comparison to the C-band reference transmission, the average C-band GSNR has reduced in the C+L and C+L+S band scenarios due to NLI and its interaction with the Stimulated Raman Scattering (SRS) effect. The lightpaths are assigned based on the defined routing and wavelength assignment (RWA) algorithm ($k$-shortest paths with $k_{max} = 5$ for routing and first-fit for spectrum allocation) and the characteristics of the ZR+ transceiver [13]. Moreover, the network assessment is done using a uniform traffic distribution among the network nodes. This work considered the Spain-E topology consisting of 30 optical nodes and 52 edges with an average node degree of 3.46 as shown in Fig. 8. Network metrics are statistically determined by Monte Carlo analysis.

## V. Results and Conclusion

To compare the multiband results when using the ROADM architecture with the proposed WSS structure, we compare the BDM to SDM network performance, assuming that SDM uses multiple fibers within the C-band on the same total available spectrum. For SDM, we assume a core continuity constraint (CCC) where each LP from the source to the destination node must be allocated in the same fiber, which corresponds to the switching technique [14]. This option is preferable because it increases the number of fiber pairs by two or three times compared to the BDM approach with S+C+L. SNAP is applied to both ideal (penalty-free) and realistic ZR+ transceivers. We consider the C-band 1x fiber as a reference and compare (i) the C-band SDM 2x fibers with the C+L BDM, (ii) the C-band SDM 3x fibers with the S+C+L BDM. Results in Fig. 10 are presented as a statistical average over Monte Carlo runs of the blocking probability (BP) versus total progressively assigned traffic for each BDM and equivalent SDM scenario. Using $BP = 10^{-2}$ as a reference, we determine the amount of traffic that can be allocated for each case: this is the comparison metric for the different transmission solutions. The dotted line represents the ideal transceiver case whereas the plain line shows the ZR+ transceiver case. When comparing BDM and SDM solutions, for both ideal and realistic ZR+ transceivers, we found that all BDM solutions are very close to their respective SDM reference solution.

Fig. 11 (a), (b) shows deployed traffic comparison of SDM (C-band, 2x fibers) against BDM (C+Lband, 1x fiber). Fig. 11 (c), (d) shows deployed traffic comparison of SDM (C-band, 3x fibers) against BDM (S+C+Lband, 1x fiber). Deployed traffic is represented in the form of an heat map where dark orange color shows larger traffic deployment and blue color shows less traffic deployment. The deployed traffic per link for the case of BDM is slightly less than the SDM case which require 2x or 3x additional fibers deployment. In Fig. 11 (a), the traffic deployment for SDM case is 3.3% greater than the BDM shown in Fig. 11 (b). Whereas, in Fig. 11 (c) and (d), the difference between SDM and BDM traffic deployment is arround 11.8%. For the later scenario, the difference is larger due to the non-linear propagation penalty introduced by transmitting three bands (S+C+L) on a single fiber. The BDM scenario (C+L, S+C+L) increases the capacity of the Spain-E network by around double and triple compared to the C-band solution (1x fiber - reference). SDM solutions provide slightly more traffic than BDM due to the non-linear propagation penalty of providing all channels in the same fiber in case of BDM. It is possible to improve BDM and minimize this difference by properly adjusting the transmit power for each band, an approach we have not considered in this work. In any case, BDM shows no significant reduction in capacity, and it proves to be a potentially cost-effective technology for upgrading network capacity without the need to install new fibers.

## References

[1] A. Napoli, N. Costa, J. K. Fischer, J. Pedro, S. Abrate, N. Calabretta, W. Forysiak, E. Pincemin, J. P.-P. Gimenez, C. Matrakidis *et al.*, "Towards multiband optical systems," in *Photonic Networks and Devices,* (Optical Society of America, 2018), pp. NeTu3E–1.

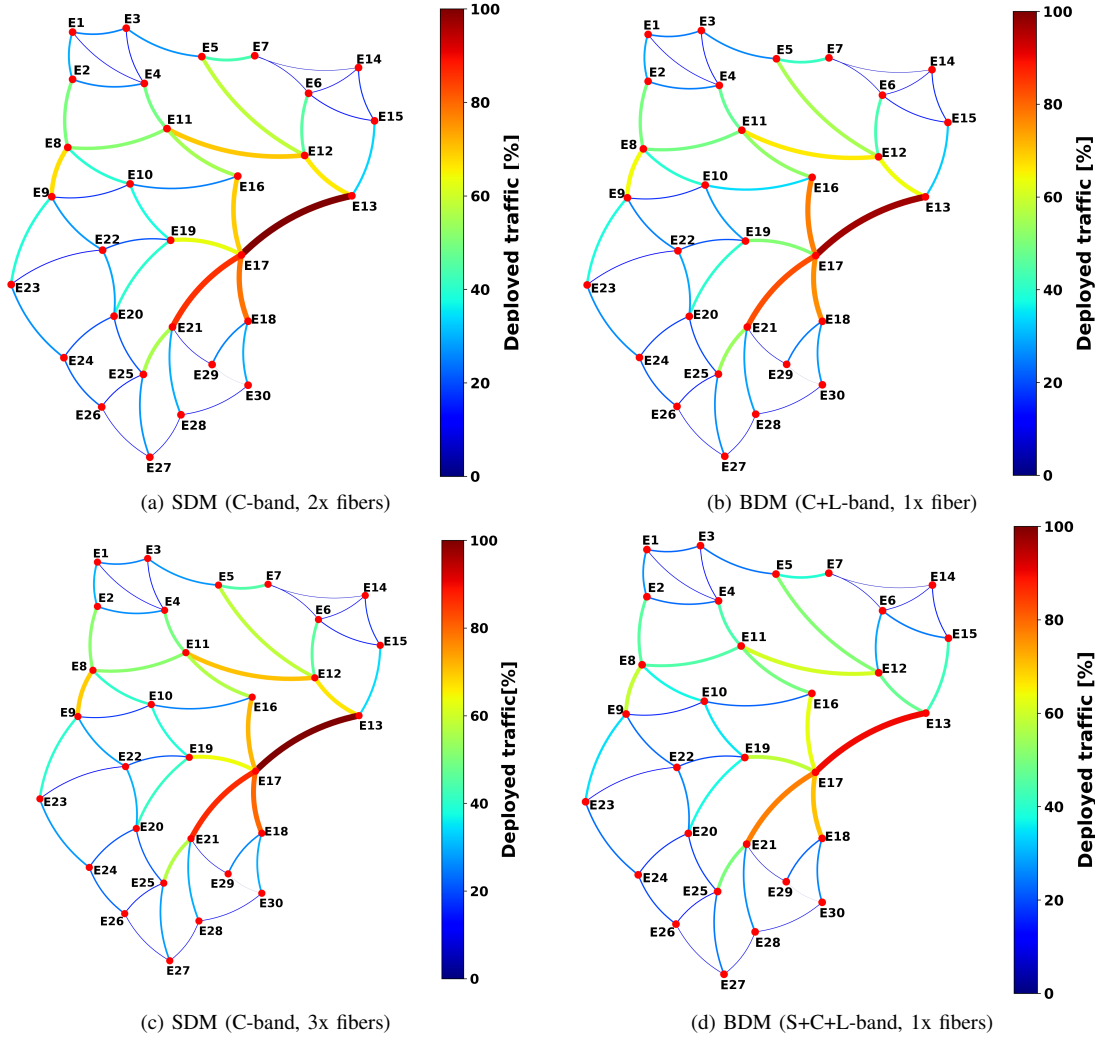


(a) SDM (C-band, 2x fibers)

(b) BDM (C+L-band, 1x fiber)

(c) SDM (C-band, 3x fibers)

(d) BDM (S+C+L-band, 1x fibers)

Fig. 11. Deployed traffic comparison - ZR+ transceiver.


[2] K. Kim, K.-H. Doo, H. H. Lee, S. Kim, H. Park, J.-Y. Oh, and H. S. Chung, "High speed and low latency passive optical network for 5G wireless systems," JLT **37**, 2873–2882 (2018).

[3] A. Ferrari, A. Napoli, J. K. Fischer, N. Costa, A. D'Amico, J. Pedro, W. Forysiak, E. Pincemin, A. Lord, A. Stavdas *et al.*, "Assessment on the achievable throughput of multi-band ITU-T G. 652. D fiber transmission systems," J. Light. Technol. **38**, 4279–4291 (2020).

[4] V. Curri, "Multiband optical transport: a cost-effective and seamless increase of network capacity," in *PND,* (OSA, 2021), pp. NeTu2C–3.

[5] T. A. Strasser and J. L. Wagener, "Wavelength-selective switches for roadm applications," IEEE JSTQE **16**, 1150–1157 (2010).

[6] M. Hammood, A. Mistry, H. Yun, M. Ma, S. Lin, L. Chrostowski, and N. A. F. Jaeger, "Broadband, silicon photonic, optical add–drop filters with 3 dB bandwidths up to 11 THz," OL **46**, 2738–2741 (2021).

[7] X. Tu, C. Song, T. Huang, Z. Chen, and H. Fu, "State of the art and perspectives on silicon photonic switches," Micromachines **10** (2019).

[8] I. Khan, L. Tunesi, M. U. Masood, E. Ghillino, P. Bardella, A. Carena, and V. Curri, "Optimized management of ultra-wideband photonics switching systems assisted by machine learning," Opt. Express **30**, 3989–4004 (2022).

[9] I. Khan, L. Tunesi, M. U. Masood, E. Ghillino, P. Bardella, A. Carena, and V. Curri, "Machine learning assisted accurate estimation of qot impairments of photonics switching system on 400zr," in *ACP 2021,* (Optica Publishing Group, 2021), p. T2B.2.

[10] V. Curri, M. Cantono, and R. Gaudino, "Elastic all-optical networks: A new paradigm enabled by the physical layer. How to optimize network performances?" JLT **35**, 1211–1221 (2017).

[11] B. Correia, R. Sadeghi, E. Virgillito, A. Napoli, N. Costa, J. Pedro, and V. Curri, "Power control strategies and network performance assessment for C+L+S multiband optical transport," JOCN **13**, 147–157 (2021).

[12] V. Curri, A. Carena, A. Arduino, G. Bosco, P. Poggiolini, A. Nespola, and F. Forghieri, "Design strategies and merit of system parameters for uniform uncompensated links supporting Nyquist-WDM transmission," JLT **33**, 3921–3932 (2015).

[13] Implementation agreement for a 400ZR coherent optical interface, https://www.oiforum.com/technical-work/hot-topics/400zr-2/.

[14] P. S. Khodashenas, J. M. Rivas-Moscoso, D. Siracusa, F. Pederzolli, B. Shariati, D. Klonidis, E. Salvadori, and I. Tomkos, "Comparison of spectral and spatial super-channel allocation schemes for sdm networks," JLT **34**, 2710–2716 (2016).